Check for updates

Reinforcement using undoped carbon quantum dots (CQDs) with a partially carbonized structure doubles the toughness of PVA membranes†

Zeeshan Latif, [ID] [a] Hasan B. Albargi, [ID] [bc] Zubair Khaliq, [ID] [a] Kinza Shahid,[a] Usama Khalid,[a] Muhammad Bilal Qadir, [ID] *[d] Mumtaz Ali, [ID] *[d] Salman Noshear Arshad, [ID] [e] Ali S. Alkorbi [ID] [f] and Mohammed Jalalah [ID] [cg]

Nano-carbon-reinforced polymer composites have gained much consideration in functional applications due to their attractive mechanical strength and cost-effectiveness. The surface chemistry and associated mechanical strength of carbon nanotubes (CNTs), graphene, and other carbon derivative-based nanocomposites are well understood. While CQDs are considered emerging carbon derivatives, their surface chemistry, unique physio-chemical properties, and dispersion behavior in polymers are yet to be explored. Therefore, in this work, CQDs with different structures were synthesized from lemon pulp and urea, and their rheology and mechanical strength were studied in the PVA matrix. The surface chemistry and structure of CQDs were controlled using different solvents and reaction temperatures, respectively. CQDs possessed a circular shape, with a size of <10 nm, having a suitable carbon core and functional groups, as confirmed by TEM and FTIR spectroscopy. The dynamic viscosity and particle size of PVA/CQDs films peaked at 4% inclusion due to the maximum crosslinking of U-CQDs with reinforcement at 180 °C. Compared with pure PVA, the optimized composite showed an 80% larger particle size with 67% better tensile strength at 4% U-CQDs concentration. In addition to enhanced mechanical strength, CQDs exhibited antibacterial activity in composites. These CQDs-reinforced PVA composites may be suitable for different functional textile applications (shape memory composites and photo-active textiles).

Introduction

Carbon nanomaterials include a variety of carbon derivatives with different shapes and sizes, which make them suitable for a broad range of applications.[1] The most recent derivative of carbon materials is carbon quantum dots (CQDs), which serve as cost-effective and sustainable nano-reinforcements for mechanical and functional applications.[2] CQDs consist of an amorphous and crystalline carbon mixture as the core along with a highly functional surface and typically have a size of less than 10 nm.[3] The structure of CQDs allows the tunability of properties for specific applications, such as composites, semiconductors, and photocatalysts; besides, CQDs serve as sustainable precursors and involve facile synthesis. Specifically, large amount of CQDs required for nano-reinforcement of polymers can be achieved by a bottom-up approach *via* carbonization of organic precursors. The formation of CQDs includes four stages: (1) homogenous mixing of precursors, (2)

[a]*Department of Materials, School of Engineering and Technology, National Textile University, Faisalabad 37610, Pakistan. E-mail: zeeshanlatif203@yahoo.com; zubntu@yahoo.com; kinzashahid1560@gmail.com; usamakhalidqurashi@gmail.com*

[b]*Department of Physics, Faculty of Science and Arts, Najran University, Najran 11001, Saudi Arabia. E-mail: hbalbargi@nu.edu.sa*

[c]*Advanced Materials and Nano-Research Centre (AMNRC), Najran University, Najran 11001, Saudi Arabia. E-mail: msjalalah@nu.edu.sa*

[d]*Department of Textile Engineering, School of Engineering and Technology, National Textile University, Faisalabad 37610, Pakistan. E-mail: bilal_ntu81@hotmail.com; mumtaz.ali@ntu.edu.pk*

[e]*Department of Chemistry and Chemical Engineering, Lahore University of Management Sciences, Lahore 54792, Pakistan. E-mail: salman.arshad@lums.edu.pk*

[f]*Department of Chemistry, Faculty of Science and Arts at Sharurah, Najran University, Sharurah 68342, Saudi Arabia. E-mail: assalem@nu.edu.sa*

[g]*Department of Electrical Engineering, College of Engineering, Najran University, Najran 11001, Saudi Arabia*

formation of fluorophore molecules, (3) formation of a more extensive molecular network, and (4) partial carbonization of molecular networks into CQDs. The transformation of precursors to CQDs is a temperature-driven process; therefore, an elevated temperature is required for their synthesis *via* hydrothermal, magnetic hyperthermia, microwave, plasma, and ultrasonic routes. The properties of CQDs formed by these synthetic methods can be tuned by controlling the temperature and reaction time, as well as the degree and time of carbonization. At the same time, the type of organic precursors is also an important parameter.[4]

The size, degree of carbonization, and functional groups at the surface of CQDs can influence the properties of CQDs-embedded polymer composites. The addition of CQDs changes the crystallization dynamics, phase segregation, and crystal growth as it serves as a crosslinking agent.[5,6] In addition, CQD composites have an advantage over other nano-reinforcements as they do not require surface modifications or dispersing agents. Furthermore, their high surface area causes stress dissipation, thus enhancing the mechanical strength of the polymeric structures, *i.e.*, increasing their strength and elongation. The interaction of CQDs with polymers can be *via* chemical or physical crosslinking; the former has been shown to increase the mechanical strength by up to 100%, and the latter is capable of only 50% strength enhancement.[7] In contrast, the effect of reinforcement was more prominent in thermosetting polymers due to chemical crosslinking than in thermoplastic polymers. The addition of 0.5 wt% CQDs in a polymer resin led to a threefold increase in strength, exhibiting their remarkable ability in the synergistic enhancement of properties. Thus, mechanically enhanced polymers with CQDs can be used for structural applications.[8] In another study, functionalized graphene (f-Gr) was incorporated in PVA to obtain PVA-graphene (Gr) nanocomposite films fabricated at varying refluxing and vacuum oven times. Nitric acid (HNO_3) was used to functionalize the graphene nanoparticles. The PVA-f-Gr nanocomposite had a higher storage modulus than pristine PVA and the PVA-Gr composite across the entire temperature range, according to the dynamic mechanical analysis (DMA). The introduction of f-Gr nanocrystals into the PVA matrix had a significant impact on the glass transition state (T_g), loss modulus, and damping factor ($\tan \delta$) of the PVA-f-Gr nanocomposite films.[9] Furthermore, functionalized silicon carbide (f-SiC) nanoparticles synthesized *via* acidic oxidation with HNO_3 exhibited a homogeneous and stabilized distribution of activated silicon carbide (SiC) within the PVA chains. The PVA/f-SiC nanocomposite containing 2 wt% f-SiC showed 77% higher mechanical strength and 105% higher storage modulus.[10]

Composites of CQDs with thermoplastic polymers can be fabricated *via* physical mixing; however, this can cause compatibility problems due to the aggregation of CQDs. Therefore, chemical bonding, which involves interlinking and interfacial interactions between the polymer chains and CQDs, is preferably employed to avoid aggregation problems. A CQDs/thermoplastic polyurethane composite fabricated with 1 wt% CQDs (added during the polymerization of thermoplastic polyurethane) showed 1.5 times higher mechanical strength because of the increased number of active bonding sites on the surface of the CQDs provided by their functional groups. Increasing the content of CQDs above 1 wt% in polyurethane caused aggregation in the matrix and loss of strength due to increased brittleness.[11,12] In addition, CQDs have been used to reduce the stiffness of polyacrylonitrile (PAN)-derived carbon nanofibers. The application scope of PAN-derived carbon nanofibers is limited due to their brittleness. CQDs synthesized from coal using a nitric and sulfuric acid mixture were used to fabricate a 1 : 1 nanocomposite of CQDs:PAN nanofibers, which showed a 7 times higher young modulus. This can be explained by the increased chain alignment in the nanofibers due to the functional groups on the surface of the CQDs.[13]

A previous study used the concept of CQDs nano-reinforcement in polyvinyl alcohol (PVA) films for strength and electromagnetic applications. CQDs were synthesized using a microwave approach, and CQDs–PVA films with different concentrations were fabricated using the solution casting method. The addition of CQDs increased the breaking strength by tenfold, while the optimum concentration of CQDs was 6%. On the other hand, the inclusion of 8% CQDs decreased both strength and elongation due to aggregation.[14] The increase in Young's modulus in the optimized CQDs composites was related to the prevention of chain slippage due to increased packing density.[15] Similar results were observed for solution-cast composite films of chitosan (CS) and nitrogen–sulfur (NS) co-doped CQDs. The results showed that adding CDQs at 2 wt% enhanced Young's modulus and tensile strength by nearly 1.5 times.[16] The increase in the mechanical performance of the nanocomposite can be attributed to strong hydrogen bonding at the CS and NS-CQDs interface.[17] Another study used CQDs for the reinforcement of epoxy/polyurethane (PU) composites for multipurpose applications such as strength, flexibility, and UV protection. The pre-PU polymer and epoxy were mixed at 55 °C for 2 h. and mixed with a CQDs/DMF solution for over 2 h. The mixture was cooled at ambient temperature, and a nanofilm was created on the steel surface. Mechanical testing of the film showed that adding 3% CQDs increased its toughness by more than 100%.[18]

Previously, CQDs synthesized based on citric acid, urea, and ethylene diamine as precursors have been used in polymer matrices as reinforcement materials; however, there is less focus on sustainable biomass-derived CQDs. Furthermore, numerous studies are available on the effect of different concentrations of CQDs on polymer matrices. However, the effects of intrinsic factors of CQDs, including crystallinity, size, surface chemistry, and the mechanism related to increased tensile properties, have not been comprehensively investigated in previous studies. To understand the mechanism underlying the enhanced mechanical and functional properties of CQDs-polymer composites, the effects of CQDs structure, functional groups, and optimized concentration on CQDs–PVA composites were studied herein. CQDs were synthesized using lemon pulp as the precursor, while the functional groups were controlled using different solvents for hydrothermal carbonization. The CQD structure was tuned by using different synthesis

temperatures to alter the degree of carbonization and the associated structure of the CQDs. The rheology and mechanical strength of the CQDs–PVA composites were compared to elucidate the mechanism of the reinforcement effect of CQDs. Water was the best solvent for enhancing the mechanical strength, and the undoped structure was better than the nitrogen-doped structures. The composite structure of CQDs–PVA showed a higher degree of amorphous regions, increasing the elongation. The crosslinking effect of CQDs, as confirmed by the rheology studies, can directly be related to their enhanced mechanical strength.

Experimental methods

Materials

Polyvinyl alcohol (PVA, M.W.; 89 000 to 98 000, degree of polymerization 2023 to 2227, 95% purity) was purchased from Sigma-Aldrich (USA). Laboratory-grade solvents such as ethanol and N,N-dimethylformamide (DMF) were purchased from Sigma-Aldrich, USA. Other laboratory-grade chemicals, including citric acid and urea, were purchased from the local chemical market (Pakistan) to synthesize CQDs. A dialysis membrane with a pore size of 20 kDa was purchased from the local chemical market (Pakistan) to separate the CQDs.

Methods

Synthesis of CQDs. The CQDs were synthesized *via* a hydrothermal method using 4 g lemon pulp as the carbon precursor and 6 g urea as the nitrogen dopant (for the synthesis of nitrogen-doped CQDs). These precursors were dispersed in 30 mL of different solvents, namely deionized water, ethanol, and DMF, to synthesize nitrogen-doped CQDs denoted as W-CQDs, E-CQDs, and D-CQDs, respectively. In the case of undoped CQDs, only 4 g of lemon pulp was dissolved in 30 mL of deionized water to synthesize U-CQDs. The resulting mixtures were sonicated for 15–20 min in a water bath sonicator at room temperature to disperse the reactants. The dispersed solutions were poured into a 100 mL hydrothermal reactor for carbonization. The hydrothermal reactor was placed in an oven at 140 °C, 180 °C, and 220 °C for 6 h to obtain CQDs of different sizes and structures. After carbonization, a dialysis membrane was used to separate the nanoparticles based on their sizes. After purification, the colloids of CQDs were dried at 80 °C in an oven.

PVA/CQDs nanocomposites. PVA/CQDs nanocomposite films were fabricated using the solution casting technique. A hot-plate magnetic stirrer was used to prepare the PVA/CQDs nanocomposite solution. First, 8 g PVA was dissolved in 40 mL distilled water for 12 h at 70 °C. After that, CQDs at different concentrations with respect to PVA, such as 2, 4, and 6 wt%, were added to the PVA solution. The prepared solutions were poured onto molds and left for 1 day at room temperature to evaporate the water. All the films were fabricated using a film applicator while maintaining a slow heating rate for solvent evaporation. Fast heating may result in the formation of voids or trapped air bubbles. The PVA/CQDs nanocomposite films were characterized using different characterization techniques.

The average tensile strengths of samples (5 replicates) fabricated with different surface chemistry, size, structure, and concentration of CQDs in the PVA polymer were compared (Table S1†).

The experimental design of the synthesis of CQDs and the fabrication of nanocomposites is shown in Scheme 1. Initially, the different surface states of the CQDs were optimized by using various solvents (water, ethanol, and DMF) in the hydrothermal process. Undoped CQDs were also synthesized in water. The solvent that offered the optimized surface state was used to carbonize the CQDs at different temperatures, *i.e.* 220 °C, 180 °C, and 140 °C. Finally, the optimal concentration of CQDs in PVA was determined by testing 2%, 4%, and 6% of CQDs in the composite structure.

Characterization

The chemical composition of all the synthesized CQDs was confirmed using Attenuated total reflection Fourier transform infrared spectroscopy carried out on an ASTM E168 (ATR-FTIR; Spectrum Two, PerkinElmer, Germany). Photoluminescence spectroscopy (Jobin Yvon HORIBA NanoLog, France) was used to analyze the Stoke shifts of the CQDs. A UV-vis spectrophotometer (LAMBDA 950, PerkinElmer, United Kingdom) was used to identify the electronic structure of the CQDs. The structural crystallinity of the PVA/CQDs nanocomposites was analyzed using X-ray diffraction (XRD; X′ Pert Pro, PANalytical, Netherland) with a PIXcel detector and Cu Kα radiation in the $2\theta = 10–50°$ range and a 2θ step size of 0.03. A zeta sizer was employed to confirm the particle size by dynamic light scattering according to ISO 13322-2: 2021 and ISO 22412. The mechanical testing of the PVA/CQDs nanocomposites was performed using a Universal testing machine ASTM D 5079 (UTM; Zwick/Roell Z100, Germany). For tensile testing, samples of length 130 mm and width 25 mm were prepared. The morphology, crystal lattice, and size of the optimized CQDs were confirmed by transmission electron microscopy (TEM; JEM-2100F, JEOL Ltd, Japan). The antibacterial activities of pure PVA and the PVA–CQDs nanocomposites were evaluated after 0 and 24 h using the agar diffusion method according to the ISO-20743 standard test.

Results and discussion

The formation of solvent-induced surface states in CQDs in the presence of various solvents is shown in Fig. S1.† The solvents also contribute to the reaction and form new functional groups. The reaction is accomplished in three steps: (i) rearrangement of the reactants, (ii) condensation reaction to produce fluorophores, and (iii) carbonization (Fig. S1†). The exact chemical composition of CQDs is still a matter of debate; however, CQDs are assumed to have a mixture of amorphous and crystalline carbon cores, which are enriched with functional groups on the surface. The chemical structures of all undoped and N-doped CQDs, including water-based, ethanol-based, and DMF-based CQDs, are shown in Fig. S2† along with the condensation and carbonization stages.

Different surface states
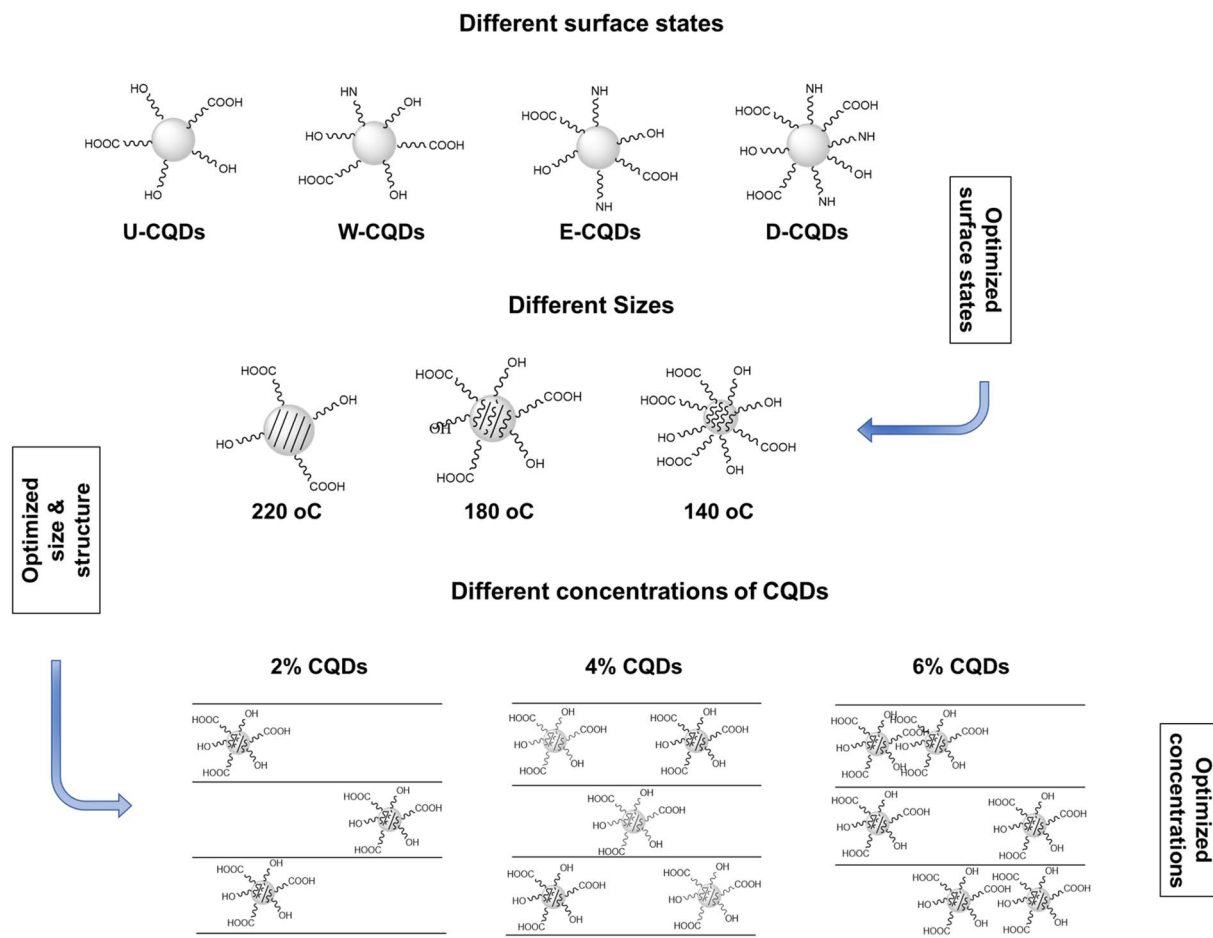
Scheme 1 Experimental design showing the stages of CQDs synthesis optimization. Initially, the surface states were compared, followed by the optimization of temperature and concentration of CQDs in the composite structure.

Fourier transform infrared (FTIR) spectroscopy

FTIR spectroscopy was performed in the attenuated total reflection (ATR) mode using a zinc selenide grid to analyze the chemical compositions of U-CQDs, W-CQDs, E-CQDs, and D-CQDs in powder form according to the ASTM E168 standard test method (Fig. 1). As seen in the figure, the stretching vibrations of the –OH (hydroxyl) and C–H (alkyl) functional groups were found at wavenumbers 3350 and 2975 cm^{-1}, respectively, in all the CQDs. However, the spectrum of U-CQDs showed broad stretching peaks of –OH and C–H, and the stretching vibrations of the H–C=O (aldehyde) groups appeared at 2675 cm^{-1} in the U-CQDs and D-CQDs IR spectra. The sharp peaks of the C=O (carbonyl) and H–O–C=O (carboxy) groups were found at 1750 and 1375 cm^{-1}, respectively, in all the CQDs spectra. The stretching vibrations of the –C–O–NH (amide) groups were seen at 1275 cm^{-1} in the spectra of nitrogen-doped CQDs, such as W-CQDs, E-CQDs, and D-CQDs. No nitrogen functional groups available were present in undoped CQDs, namely U-CQDs. In addition, the IR signals of the C–O–C (ether) groups were noted at 1175 cm^{-1} for all CQDs. In addition, the stretching vibrations of D-CQDs showed that the content of oxygenated and nitrogenated groups was higher than

those in the other nitrogen-doped CQDs, namely W-CQDs and E-CQDs.

Optical characterization

The optical properties of the CQDs were analyzed to confirm the synthesis of CQDs with different surface states. The change in surface states was observed from the Stokes shift of the CQDs. UV-vis spectroscopy was used to study light absorption by the CQDs and the associated electronic transition in the UV and visible spectral range. The absorbance spectra of U-CQDs, W-CQDs, E-CQDs, and D-CQDs were analyzed using a UV-vis spectrophotometer, and the results are shown in Fig. 2(a). The UV-vis absorbance spectra displayed two regions: one for π–π* transitions in the 250–380 nm wavelength range of the UV spectrum, and the second representing n–π* transitions in the visible 380–700 nm wavelength spectrum. The π–π* higher energy spectrum is associated with the carbon cores (C–C, C=C), and these peaks were found in all samples, including U-CQDs, W-CQDs, E-CQDs, and D-CQDs.[19] Meanwhile, n–π* in the lower energy spectrum is associated with the surface states, which generate discrete energy levels between the highest occupied molecular orbitals (HOMOs) and the lowest
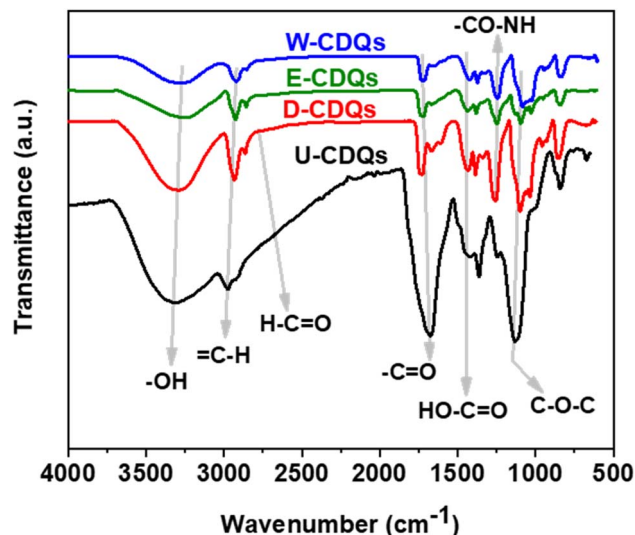
Fig. 1 FTIR spectra show that undoped CQDs have only oxygenated functional groups and nitrogen-dopped CQDs have both oxygenated and nitrogenated functional groups.

unoccupied molecular orbitals (LUMOs).[19,20] Two types of surface states could be observed: (1) oxygenated functional groups such as C=O or C–O were observed in all CQDs. (2) Nitrogenated functional groups such as C–N–C or C–N–H occurred in nitrogen-doped CQDs such as W-CQDs, E-CQDs, and D-CQDs. The shoulder peaks of the nitrogen-doped CQDs indicate that the content of both oxygenated and nitrogenated functional groups was higher in D-CQDs.[21] The E-CQDs showed a broad peak of oxygenated groups; however, the content of nitrogenated groups was lower than that in W-CQDs. The shoulder peaks of the undoped U-CQDs represented only oxygenated functional groups. Generally, a higher number of surface functional groups decreases the HOMO–LUMO energy gap, resulting in transitions at lower energies.[22,23] The change in the excitation energy values was calculated using Tauc plots, and the HOMO–LUMO bandgaps of U-CQDs, W-CQDs, E-CQDs, and D-CQDs were calculated to be 2.48, 2.39, 2.37, and 2.32 eV, respectively [Fig. 2(b)].

Fluorescence is an optical characteristic of CQDs that can be directly related to their electronic structure. The PL spectra verified the quantum confinement effect and related photoexcitation in the CQDs. The characteristic emission of the CQDs in the colloid state was analyzed after excitation using PL spectroscopy, which exhibited their excitation-emission spectra. The emission of the U-CQDs, W-CQDs, E-CQDs, and D-CQDs colloids were centered at wavelengths 440, 450, 475, and 550 nm, respectively [Fig. 2(c)]. An increase in the surface state usually causes a decrease in the bandgap between the HOMO and LUMO levels; therefore, the Stokes shifts increase.[24,25] The D-CQDs revealed the highest content of surface states. Consequently, the bandgap between its HOMO and LUMO levels was the least. As the bandgap decreases, discrete energy levels are formed between HOMO and LUMO levels; therefore, the PL spectra showed emission at higher wavelengths.[26,27] Based on

the UV-vis absorbance spectra and bandgap values, the possible electronic transitions of the CQDs are shown in Fig. 2(d). The undoped CQDs have the least surface states and vibrational relaxation; therefore, they have the largest band gap and low Stokes shift emission. Compared with E-CQDs and W-CQDs, the surface states and vibrational relaxation of D-CQDs are higher; therefore, the bandgap of D-CQDs would be decreased, hence resulting in higher Stokes shift emission. Equivalent representations of CQDs HOMO–LUMO changes have been reported in previous studies.[21,28–32] The colloids of U-CQDs, W-CQDs, E-CQDs, and D-CQDs emitted blue, bluish-yellow, yellowish-green, and yellow colors under UV irradiation, respectively [Fig. 2(e)]. In addition, the emissions of pure PVA and the PVA + U-CQDs, PVA + W-CQDs, PVA + E-CQDs, and PVA + D-CQDs nanocomposite films were observed under UV and visible lights, as shown in Fig. 2(f). The emission of the D-CQDs films was the highest under the UV irradiation, which represents their high quantum yield and better dispersion in the PVA matrix. However, the emission of U-CQDs was almost quenched after dispersion in the PVA matrix.

Optimization of the different surface states of CQDs

The effects of the different surface states of CQDs on the mechanical and rheological properties of the PVA/CQDs nanocomposites were analyzed, as shown in Fig. 3. The average particle sizes of the PVA/CQDs nanocomposites with different surface states of CQDs were measured using dynamic light scattering analysis (zeta sizer). As shown in Fig. 3(a), the average particle size of PVA + U-CQDs, PVA + W-CQDs, PVA + E-CQDs, and PVA + D-CQDs were observed to be 21.5, 12.5, 14, and 17 d nm, respectively. The average particle size of the PVA/CQDs composite with undoped CQDs reinforcements was greater than those of the nanocomposites fabricated using nitrogen-doped CQDs. The particle size is associated with the interaction of the CQDs with the PVA molecules; as the intermolecular interactions between PVA and CQDs increase, the average particle size of the PVA/CQDs composite increases. The nitrogen-doped CQDs have both oxygenated and nitrogenated functional groups in their structures. Both these functional groups are electronegative and tend to accept electrons from PVA, and these functional groups may lead to repulsion between PVA and CQDs, thereby decreasing the interaction between PVA and CQDs. Hence, the particle size of the nitrogen-doped PVA/CQDs is reduced. However, undoped CQDs have only oxygenated functional groups on their surfaces. These functional groups are more electronegative than nitrogenated functional groups and form strong physical interactions between PVA and CQDs, hence increasing the particle size of the corresponding PVA/CQDs composite.

The rheological properties, such as dynamic viscosity and tangent delta, of all nanocomposites reinforced with nitrogen-doped and undoped CQDs were analyzed against the angular frequency. The dynamic viscosities of all PVA/CQDs nanocomposites were different due to the different surface states of the CQDs, as shown in Fig. 3(b), at the same concentration of PVA. The dynamic viscosities of PVA + U-CQDs, PVA + W-CQDs,
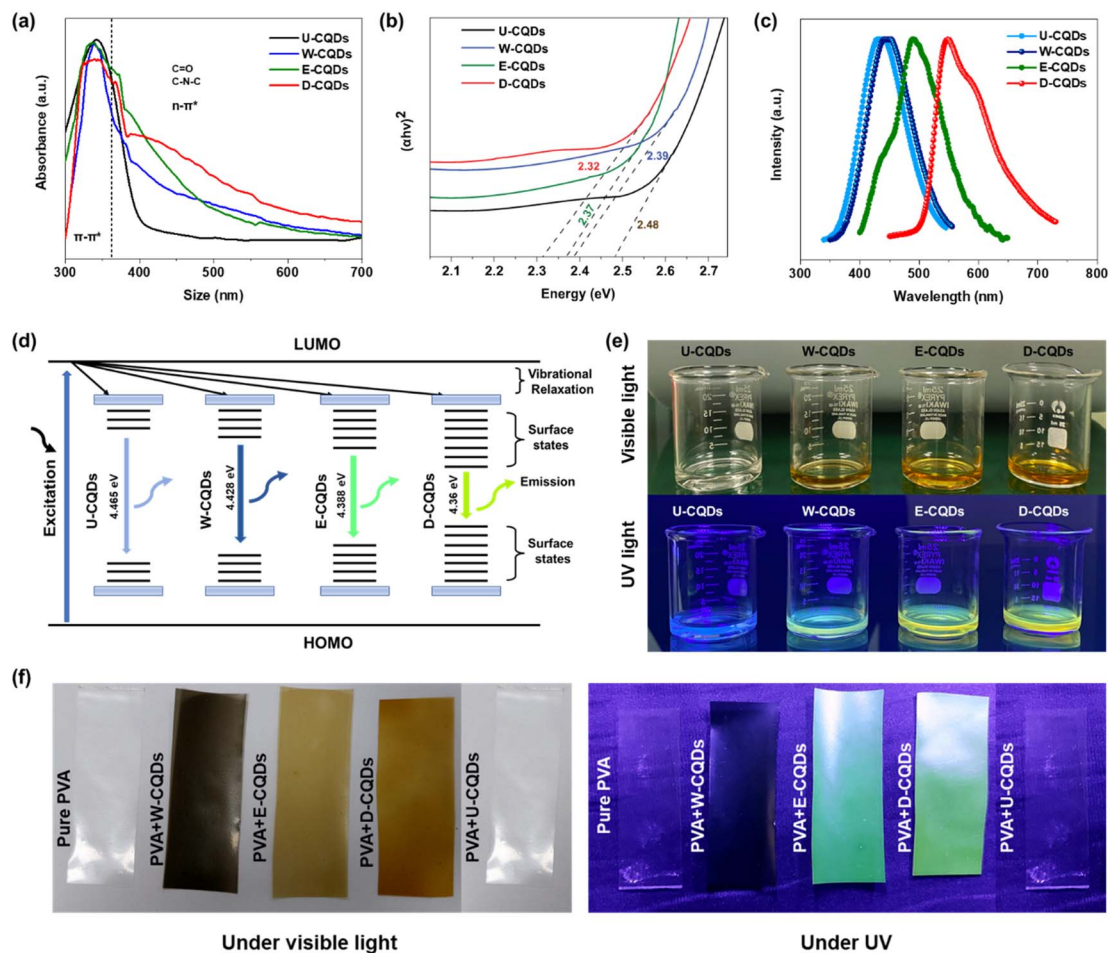
Fig. 2 Optical characterization of the CQDs colloids and CQDs–PVA composite films. (a) UV–visible absorption spectra of the undoped and nitrogen–doped CQDs colloids at 0.5% concentration. (b) Tauc plots and bandgap analysis of the CQDs colloids. (c and d) PL spectra of the CQDs and associated electronic structures. (e and f) Observation of the CQDs colloids and PVA–CQDs films under visible light and UV irradiation.

PVA + E-CQDs, and PVA + D-CQDs were found to be 10, 5, 7, and 8 Pa s, respectively. The dynamic viscosity reduced and exhibited non-Newtonian behavior as the angular frequency increased. The PVA + U-CQDs showed the highest dynamic viscosity due to the excessive content of oxygenated groups in U-CQDs, which promote excellent hydrogen bonding between the CQDs and PVA molecules. These strong intermolecular interactions produce more internal resistance between the PVA chains, resulting in its high viscosity.[33] Tangent (tan) delta is the ratio of the loss modulus to the storage modulus, and it measures the viscoelastic behavior of polymer fluids. The gel point is the state at which the sample shows viscoelastic behavior, and the tan delta is unity at the gel point. As seen in Fig. 3(c), the tan delta values of the nitrogen-doped CQDs-reinforced PVA nanocomposites were higher than that of the undoped CQDs-reinforced nanocomposite.

The storage modulus of the PVA + U-CQDs nanocomposite is enhanced due to the strong interactions of these CQDs with the polymer matrix. These strong intermolecular interactions increase the internal resistance between PVA and CQDs; hence, the viscous behavior is dominant, and the tan

delta is decreased.[18] Moreover, due to the good dispersion and better physical interactions such as hydrogen bonding and van der Waals forces between the CQDs and the PVA matrix,[34] the internal resistance between PVA and CQDs increased.[35,36]

The mechanical strength of the fabricated PVA/CQDs nanocomposite films with different CQDs surface chemistry were examined using a universal testing machine according to the ASTM D2256 standard. The tensile strength curves showing the load and extension of all the PVA/CQDs nanocomposites are depicted in Fig. 3(d). The nanocomposite films of PVA + U-CQDs, PVA + W-CQDs, E-CQDs, and D-CQDs were extended around 117%, 78%, 83%, and 76% against 122, 90, 65, and 100 N loads, respectively. The mechanical strength of the PVA/CQDs nanocomposites with U-CQDs in the polymer matrix were significantly enhanced compared with the nitrogen-doped CQDs-reinforced PVA/CQDs nanocomposites. The surface states of U-CQDs provide additional hydrogen bonding with PVA chains; therefore, the strong hydrogen bonding of PVA and CQDs enhances the mechanical strength of the PVA film.[11,26–28] The schematic of the interaction
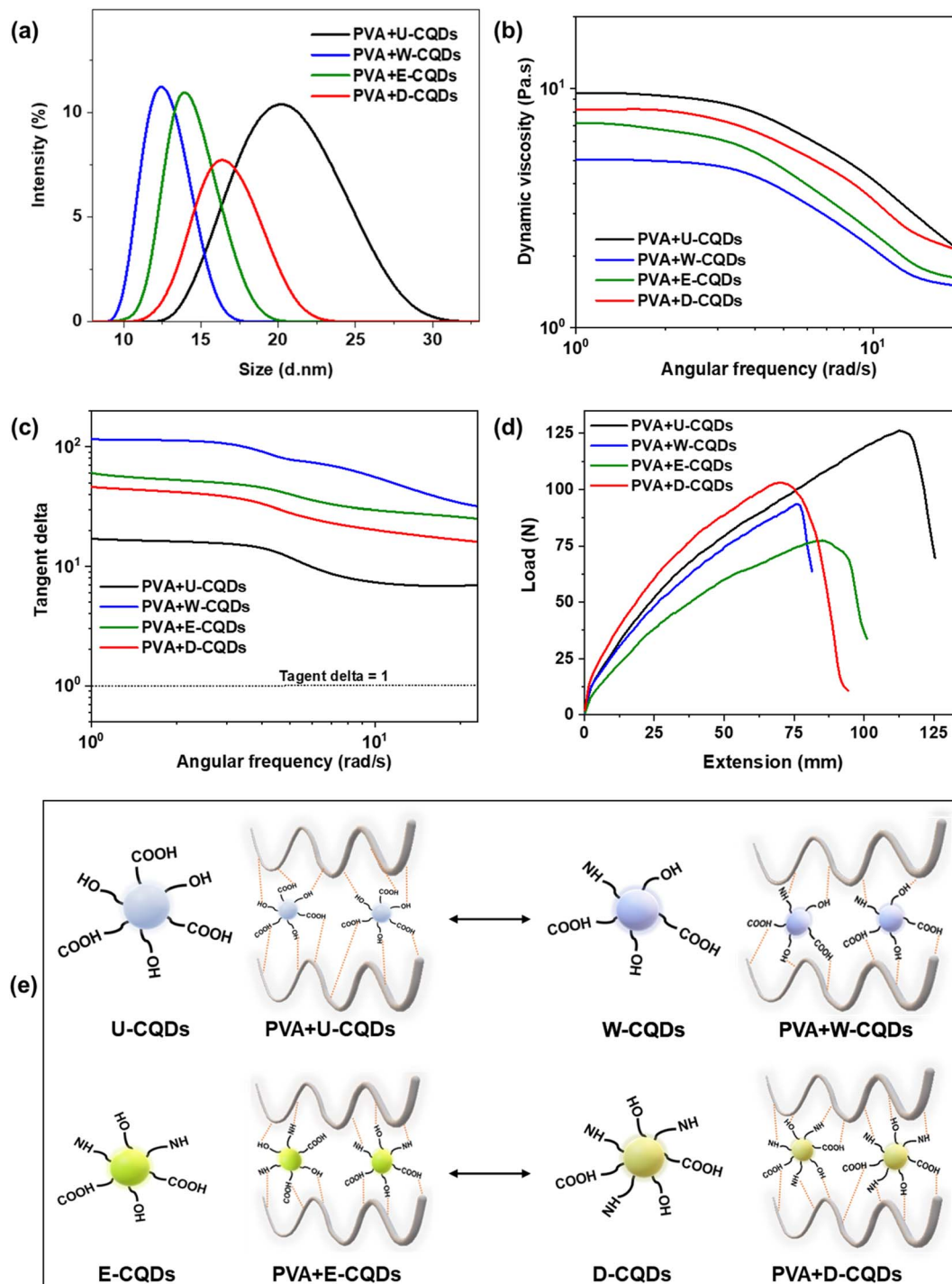
Fig. 3 Optimization of the surface states of CQDs using different solvents and nitrogen doping. Comparison of surface states *via* (a) dynamic light scattering, (b) dynamic viscosity, (c) tan-delta, and (d) tensile strength curves. (e) Postulated molecular interactions between PVA chains and the CQDs functional groups.

mechanisms in the nitrogen-doped and undoped CQDs-reinforced PVA/CQDs nanocomposites is shown in Fig. 3(e). Unlike the enhanced optical properties of nitrogen-doped CQDs, the mechanical strength of U-CQDs are better due to the stronger interactions of the electronegative oxygenated functional groups.[37–39]

Effects of the different sizes and structures of the CQDs

The effects of the different sizes and structures of CQDs on the mechanical and rheological properties of the PVA/CQDs nanocomposites were compared, as shown in Fig. 4. CQDs with different sizes and structures were synthesized by tuning the synthesis temperature. The average particle size of PVA + U-

CQDs 140 °C, PVA + U-CQDs 180 °C, and PVA + U-CQDs 220 °C were approximately 20, 21.5, and 27 d nm, respectively, as shown in Fig. 4(a). In the structure of U-CQDs 140 °C, less carbonization and higher surface functional groups that interacted with PVA molecules were observed; however, the content of carbon cores was negligible. In the structure of U-CQDs 220 °C, a higher content of carbon core and negligible content of available functional groups were found. Therefore, the size of U-CQDs 220 °C fosters weak interactions with PVA molecules. The particle size of U-CQDs synthesized at 220 °C is expected to be larger due to higher carbonization of CQDs and less functionality. Compared with this, the U-CQDs synthesized at 180 °C have both optimum surface states and carbon cores in their structures, which enabled stronger interactions with PVA. Given the suitable content of functional groups and degree of carbonization achieved in PVA + U-CQDs 180 °C, a narrow size distribution was observed in the respective composite.

The dynamic viscosity of the PVA/CQDs nanocomposites fabricated with CQDs of different sizes and structures were analyzed, as shown in Fig. 4(b). In the structure of CQDs, the carbon core provides toughness, and the functional groups offer physical crosslinking via intramolecular and intermolecular hydrogen bonding with PVA. U-CQDs 220 °C have a higher carbon core content, which provides toughness to PVA/CQDs nanocomposite; however, the functional groups are the least

due to higher carbonization at elevated temperatures. Therefore, fewer physical interactions occur between PVA and CQDs, providing less internal resistance and lower viscosity. Meanwhile, U-CQDs 140 °C have less carbon core content and higher functional groups in their structure than U-CQDs 220 °C. However, U-CQDs 180 °C have the optimum content of carbon cores and functional groups in their structure. Therefore, U-CQDs 180 °C provide higher toughness and physical crosslinking between the PVA chains. These higher molecular interactions offer higher resistance and higher viscosity. The effects of different sizes and structures of U-CQDs on the tan delta values of PVA/CQDs nanocomposites are shown in Fig. 4(c). The U-CQDs 220 °C have a lower content of functional groups, which leads to weak intermolecular interactions with PVA, and therefore, a low viscous response. U-CQDs 140 °C have a higher content of functional groups that form weak physical interactions with PVA molecules and hence have a lower viscous modulus. However, U-CQDs 180 °C have a high content of surface functional groups that produce strong physical intermolecular interactions with PVA, which can be associated with high viscous response. Therefore, the tan delta of PVA + U-CQDs 180 °C was higher than those of other CQDs.

The mechanical strength of the PVA/CQDs nanocomposites with U-CQDs of varying sizes and structures are shown in Fig. 4(d). The nanocomposites PVA + U-CQDs 140 °C, PVA + U-
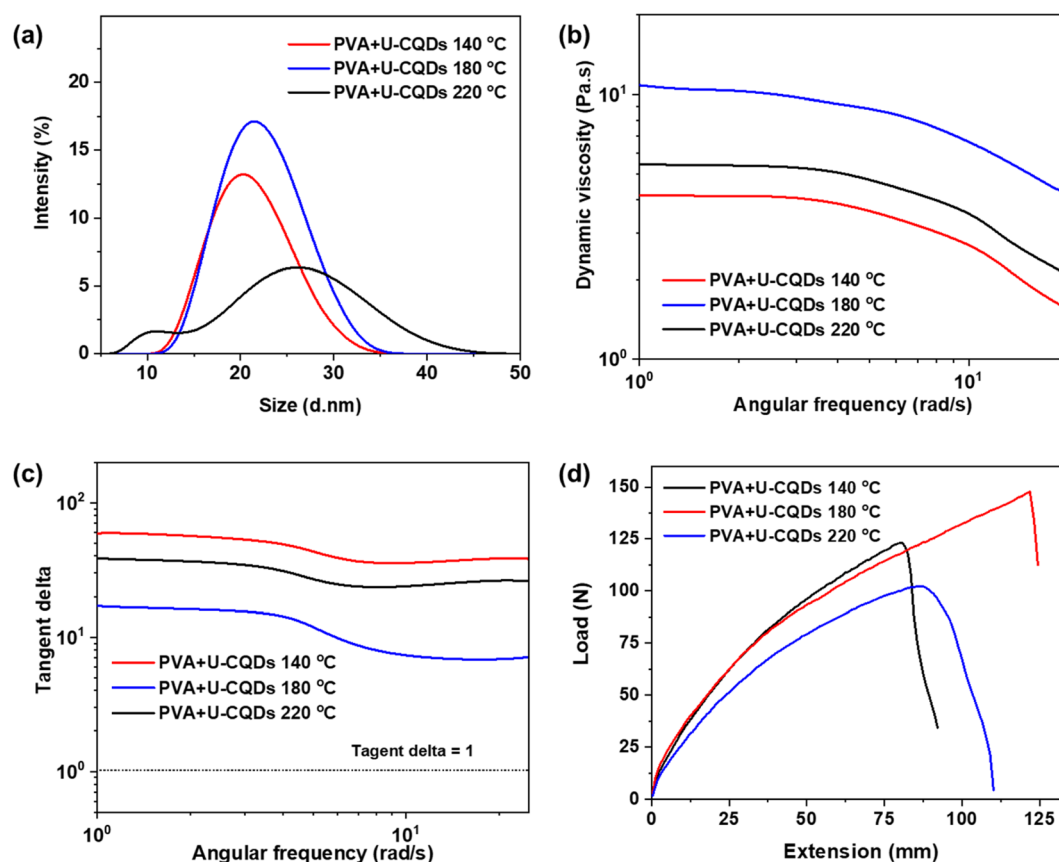

Fig. 4 Effects of different sizes and structures of optimized surface states of CQDs on PVA are shown: (a) dynamic light scattering, (b) dynamic viscosity, (c) tan-delta, and (d) tensile strength of U-CQDs synthesized at 140 °C, 180 °C, and 220 °C.

CQDs 180 °C, and PVA + U-CQDs 220 °C could elongate up to 80%, 120%, and 90% at 120, 150, and 100 N loads, respectively. The U-CQDs 140 °C reinforced nanocomposite exhibits low strength because of the poor crystal structure formed at lower temperatures, which can suppress crack generation and propagation. The U-CQDs 180 °C have suitable contents of both carbonized core structure and polar surface functional groups that offer stiffness and strong interfacial interactions between the PVA chains,[40] as required for better mechanical performance.[41] While the U-CQDs 220 °C only have good content of carbonized core structures due to high-temperature synthesis, this kind of CQDs offers fewer interactions between PVA chains and, therefore, results in composites with low strength.

Optimization of the concentration of U-CQDs 180 °C

As the U-CQDs 180 °C present the best mechanical strength, their concentration in the composite was optimized. The effects of different concentrations of U-CQDs 180 °C on the mechanical and rheological properties of PVA/CQDs nanocomposites are shown in Fig. 5. The average particle size of the PVA/CQDs nanocomposites with different optimized U-CQDs 180 °C concentrations were also analyzed, as demonstrated in Fig. 5(a). The particle size of PVA composites with 2, 4, and 6% loadings of U-CQDs were 19, 21.5, and 33.5 d nm, respectively. The average particle size of the PVA/CQDs nanocomposites with 2% loading of U-CQDs was smaller due to the lower content of active interaction sites between the PVA and CQDs. The particle size of the PVA/CQDs nanocomposites with a 4% concentration of U-CQDs was larger than that at a 2% U-CQDs concentration. At 4% U-CQDs, the maximum number of oxygenated functional groups attached to the PVA molecules produced a large particle size. As the concentration of U-CQDs increased, the particle size of the PVA/CQDs nanocomposites increased. However, at 6% loading of U-CQDs in PVA, the size of particles increased in the form of clusters because the higher content of U-CQDs caused their self-aggregation within the PVA molecules.

Fig. 5(b) depicts the effect of different concentrations of U-CQDs 180 °C on the dynamic viscosity of the PVA/CQDs nanocomposites. At 2%, 4%, and 6% U-CQDs loadings in PVA, the dynamic viscosity of the PVA/CQDs nanocomposites were 8.5, 12, and 7 Pa s, respectively. It was observed that the dynamic viscosity of the PVA/CQDs nanocomposite increased with increasing the content of CQDs. As the concentration of CQDs increased, the inter- and intra-molecular hydrogen bonding with PVA also increased, hence increasing the crosslinking density of the nanocomposite. However, at a higher content of CQDs, the dynamic viscosity of the nanocomposite was reduced due to the aggregation of CQDs in the PVA matrix. However, at 6 wt% of CQDs, the dynamic viscosity was decreased because CQDs to CQDs physical interactions were increased and formed an aggregation.[40,42] These aggregated CQDs serve as a surfactant between the PVA chains, reducing the viscosity of the nanocomposite. Fig. 5(c) shows the effect of different concentrations of U-CQDs 180 °C in PVA on the tan delta of the PVA/CQDs nanocomposites. It was observed that the tan delta of the PVA/CQDs nanocomposite decreased with increasing the

content of U-CQDs. As the concentration of U-CQDs increased, the inter- and intra-molecular hydrogen bonding with PVA also increased; hence, the crosslinking density of the nanocomposite increased. However, a very high concentration of CQDs reduces the viscous behavior of the nanocomposite due to the aggregation of CQDs in the PVA matrix.[40,43,44]

The effect of different concentrations of U-CQDs 180 °C in PVA on the mechanical strength is compared in Fig. 5(d). The results reveal that the mechanical strength of nanocomposites increased with the content of U-CQDs. As the concentration of CQDs increased, the content of active sites increased, promoting strong hydrogen bonding; hence, the mechanical strength were enhanced. However, at 6% loading of CQDs, the mechanical performance of the nanocomposite was reduced because of the self-aggregation of CQDs.[6,10,29,31,32] A schematic representation of the effect of varying the concentration of CQDs in the polymer matrix is shown in Fig. 5(e). Aggregates of CQDs disturb the intrinsic crystallization of PVA, resulting in poor mechanical strength. Due to their high surface area, CQDs can change the polymer structure even at a very low content. Consequently, higher contents are unnecessary because the maximum desirable improvement in mechanical strength can be obtained at low contents. Furthermore, the self-aggregation of CQDs observed in some past studies is due to the dissimilar hydrophobic/hydrophilic nature of the CQDs and polymers. For instance, epoxy is hydrophobic, and CQDs used as reinforcement are hydrophilic; therefore, poor mutual compatibility causes aggregation. A facile way to reduce self-aggregation is by enhancing the compatibility of the polymer matrices and CQDs reinforcements. Finally, the aggregation can be suppressed using colloidal chemistry; surface passivation of CQDs with PEG and surfactant-type polymers can be of great advantage in this regard. Similarly, highly electronegative functional groups can increase the dispersion and zeta potential of CQDs, *i.e.* fluorine-doped CQDs can potentially be tested in the future.

Comparison of pure PVA and the optimized PVA/CQDs composites

From the above results, it can be concluded that the inclusion of 4% U-CQDs 180 °C in PVA gives the best mechanical and rheological properties; a comparison of pure PVA and the optimized PVA/U-CQDs 180 °C nanocomposites is provided in Fig. 6. As shown in Fig. 6(a), the average particle size of PVA and optimized PVA/CQDs were 12 and 21.5 d nm, respectively. With the addition of 4% CQDs, the particle size of PVA/CQDs was 80% larger than that of pure PVA. The average particle size of pure PVA is smaller because of the absence of crosslinking between the PVA chains; however, the particle size of optimized PVA/U-CQDs 180 °C is larger because the CQDs serve as cross-linkers between the PVA chains.[16]

The dynamic viscosity of pure PVA and optimized PVA/CQDs are 4.1 and 12 Pa s, respectively [Fig. 6(b)], which indicate that the viscosity of PVA/CQDs was three times higher than that of pristine PVA. The carbon core and functional groups of CQDs offer strong intermolecular interactions between PVA chains, producing higher internal resistance between the chains and
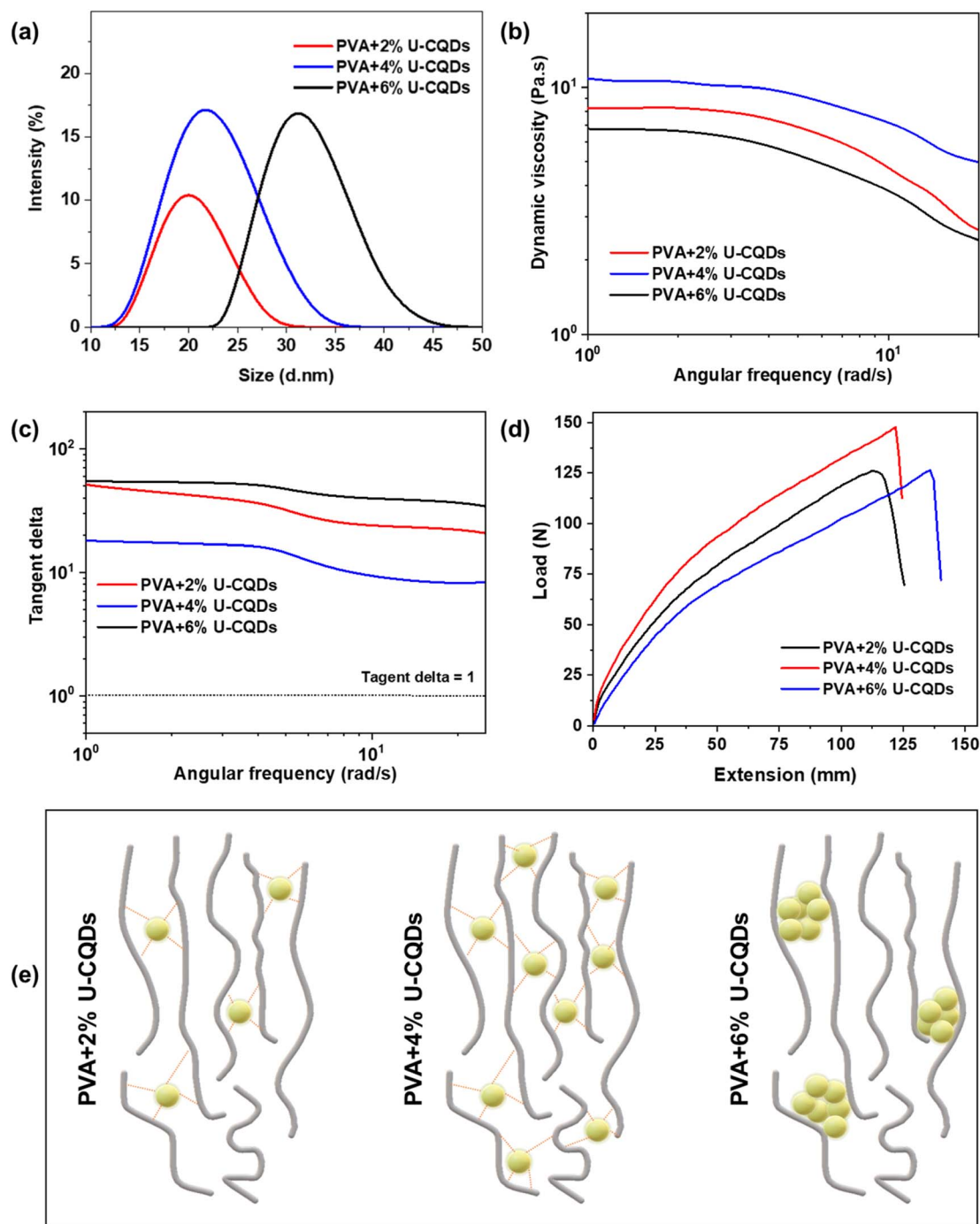
Fig. 5 Concentration optimization of U-CQDs 180 °C. Comparison of 2%, 4%, and 6% U-CQDs 180 °C loadings: (a) dynamic light scattering, (b) dynamic viscosity, (c) tan delta, (d) tensile strength and (e) schematic representation of the dispersion of CQDs at different concentrations in the PVA matrix.

thus providing higher viscosity.[33] Furthermore, the tan delta values of pure PVA and the optimized PVA/CQDs nanocomposites are compared in Fig. 6(c). The tan delta of optimized PVA/CQDs was reduced due to an increase in the viscous region of the nanocomposite, and the functional groups of CQDs provide additional crosslinking between the PVA chains.

The mechanical strength of pristine PVA and optimized PVA/CQDs are compared in Fig. 6(d); with the inclusion of 4% CQDs, the tensile strength of the nanocomposite increased by 67%

compared to that of pure PVA. The surface states of the CQDs provide additional hydrogen bonding between the PVA chains; therefore, the strong hydrogen bonding in PVA/CQDs enhanced the mechanical strength of the PVA film.[11,27,28] In addition, the CQDs have a carbonized core structure and polar surface states that offer stiffness and strong interfacial interactions between the PVA molecules,[40] which in turn lead to better mechanical performance.[41]
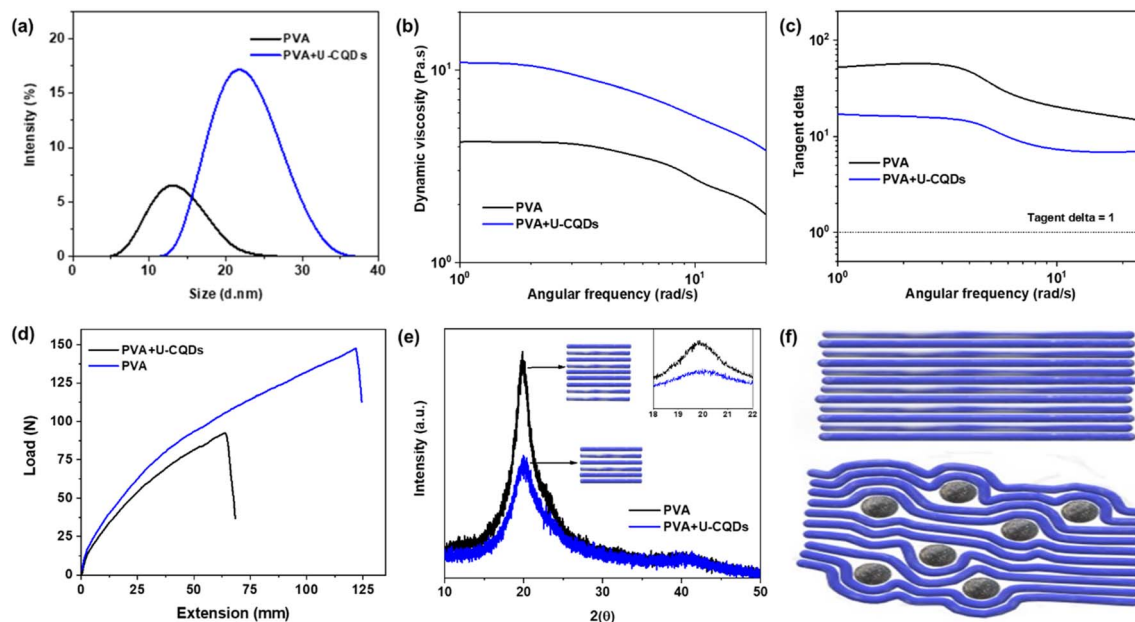
Fig. 6 Comparison of pure PVA and the PVA–U-CQDs 180 °C composite with 4% loading via (a) dynamic light scattering, (b) dynamic viscosity, (c) tan-delta, (d) tensile strength, and (e) XRD. (f) Postulated crystal structure of pure PVA and the PVA–CQD composites.

To elucidate the mechanism underlying the enhanced properties of the CQDs–PVA composite, the crystal structures of pure PVA and optimized PVA/CQDs nanocomposite were observed using XRD [Fig. 6(e)]. The broad peak of PVA was centered at $2\theta = 19.5°$ belonging to the (101) diffraction plane, which is associated with the semi-crystalline nature of the PVA polymer. However, a broad peak with lower intensity was detected for the PVA/CQDs nanocomposites at $2\theta = 20.2°$, which is attributed to the (002) diffraction plane. This difference in peak shape is associated with the highly disordered structure and higher intermolecular distance of the PVA/CQDs composite.[46] Therefore, the crystalline part of PVA was observed at a lower angle, and the crystalline part of the optimized PVA/CQDs was found at a higher angle. Furthermore, PVA has a higher-intensity peak, which is related to the higher ratio of crystalline regions. Pure PVA has a higher crystal size due to strong inter/intramolecular hydrogen bonding between the molecular chains of PVA. In contrast, the PVA/CQDs composite has smaller crystalline regions because the CQDs restrict the formation of larger-sized crystals due to the intercalation of CQDs between the PVA chains. The PVA/CQDs have a smaller crystal size because the CQDs suppress the growth of PVA crystallization [Fig. 6(f)], and therefore, empty spaces are formed. It can be said that composite films have more amorphous regions, which aids the extension of the PVA–CQDs films.

The size and structure of the optimized CQDs were analyzed using transmission electron microscopy (TEM). The structure and size of CQDs are primarily dependent on the reaction temperature, time, and precursor content.[47] At low resolution [Fig. 7(a)], the size of the optimized CQDs was found to be less than 10 nm. However, at high resolution [Fig. 7(b)], the average size of CQDs was around the range of 5 nm. The optimized

CQDs were semi-crystalline in structure with defined crystal fringes in the core and amorphous regions on the surface. The surface states on the surface of the carbon core showed amorphous domains, and the carbon core revealed the crystalline domains of the CQDs.

The quantitative antibacterial activity of pure PVA (ref.) and the nanocomposites of PVA + undoped CQDs and PVA + N-doped CQDs were analyzed after incubation times of 0 and 24 h, as shown in Fig. 8. For this purpose, agar plates were inoculated by adding a bacterial culture at 2×10^6 CFU mL^{-1} to facilitate bacterial growth. The sample was cut to 3.8 cm and autoclaved for 15 min at 121 °C. The pure PVA and PVA/CQDs nanocomposite films were placed on agar plates that were already filled with 1 mL of the bacterial solution for 60 s, and the sample surfaces were pressed down by applying a 200 g weight. Subsequently, the samples were removed from the agar surface and immediately placed in glass plates containing 30 mL water. After that, the plates were placed at 37 °C for 24 h to obtain the bacterial count at 0 and 24 h. As shown in Fig. 8, ref. $_{0\,h}$ exhibited 99.99% bacterial growth on pure PVA film, whereas ref. $_{24\,h}$ showed above 95% bacterial growth. However, the PVA + Undoped CQDs nanocomposite showed 90% bacterial growth at 0 h and 70% bacterial inhibition after 24 h. On the other hand, the nanocomposite of PVA + N-doped CQDs exhibited less than 40% bacterial growth at 0 h and almost negligible bacterial incubation after 24 h. The incorporation of N-CQDs enhanced the antibacterial activity compared with the undoped CQDs-based nanocomposite and pristine PVA as the N-CQDs offer stronger photosensitization for the production of reactive oxygen species (ROS), such as $O_2^{\bullet-}$, O_2, and HO_2^-, under light irradiation.[48–50] In addition, the N-doped CQDs absorb more light than the undoped CQDs, which is one of the main reasons

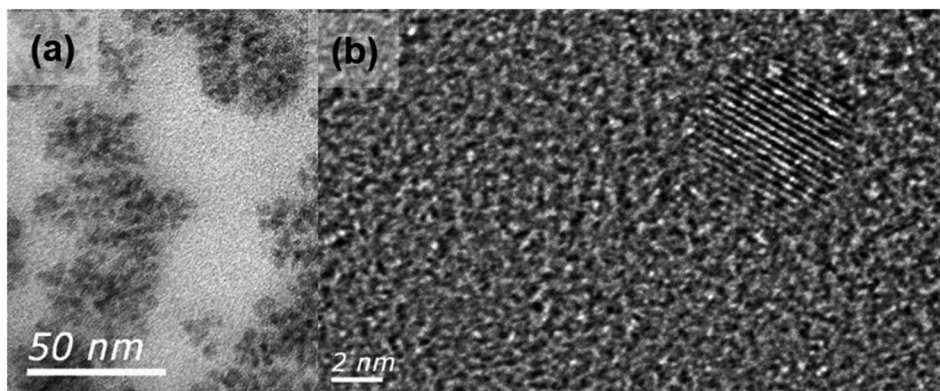© 2024 The Author(s). Published by the Royal Society of Chemistry

Fig. 7 TEM analysis of U-CQDs 180 °C shows the size and crystallographic images at (a) low resolution and (b) high resolution.

for the enhanced antibacterial activity of PVA + N-doped CQDs nanocomposite.[45] This confirms that N-CQDs not only serve as mechanical reinforcement but also impart functional attributes.[44,45]

Results from previous works and this study, including the degree of polymerization of PVA, CQDs precursors, CQDs synthesis conditions, CQDs concentration, and the mixing method of CQDs, were compared (Table S2†). However, the role of CQDs in the mechanical reinforcement of PVA has rarely been studied earlier.

Mechanisms underlying the enhancement of rheological and mechanical strength

CQDs serve as crosslinkers and enhance the viscosity of polymer materials if chemical or secondary bonds are formed between the polymer chains and CQDs. On the contrary, CQDs can serve as a lubricant in the presence of long-chain hydrocarbon molecules such as PEG, which have fewer interactions with CQDs. Unlike other nano-reinforcements, surface modification and dispersing agents are not necessary for CQDs. Furthermore, the higher surface area of CQDs offers a larger interface for stress dissipation and is, therefore, responsible for improved mechanical strength. Generally, CQDs enhance attributes related to toughness, such as tensile strength and extension, in polymer/CQDs nanocomposites. A higher elongation at break is associated with a lower degree of crystallinity of the composite, which decreases the stiffness. An enhancement in breaking load happens because of the additional crosslinks of the CQDs surfaces with the polymer matrix, which enables the carbon cores of the CQDs to overcome crack propagation. The

Fig. 8 Comparison of the antibacterial activity of pure PVA (ref.) and the PVA + undoped CQDs and PVA + N-doped CQDs nanocomposites at 0 and after 24 h of incubation.

interactions between CQDs and PVA chains are shown in Fig. (S3†). Hydrogen bonding is possible between the hydroxyl groups of PVA and CQDs, which render strong physicochemical interactions for reinforcement effect. As for the effect of CQDs doping, undoped CQDs with higher electronegativity provide suitable compatibility with most polymer materials. On the other hand, nitrogen-doped CQDs offer higher compatibility with polymers that contain highly electronegative functional groups, such as chloroprene rubber, in which nitrogen-doped CQDs can serve as the electropositive component for mutual secondary bonding.

Conclusion

CQDs were successfully synthesized from lemon pulp and urea, and their rheology and mechanical strength were studied in the PVA matrix. The CQDs possesses a circular shape, with a size of less than 10 nm, having a suitable carbon core and functional groups, as confirmed using TEM and FTIR analysis. The U-CQDs showed better performance than all nitrogen-doped CQDs and presented a moderate degree of carbonization at 180 °C temperature. The optimal content of CQDs in the PVA films was found to be 4%; lower concentrations offered fewer available functional sites, whereas higher concentrations presented the problem of aggregation. In addition, the dynamic viscosity and particle size of the PVA/CQDs film peaked at 4% inclusion when the maximum crosslinking was achieved with U-CQDs 180 °C reinforcement. Compared with pure PVA, the optimized composite with 4% U-CQDs showed an 80% larger particle size and 67% better tensile strength. The better elongation of the composite was related to the smaller-sized crystalline regions and more amorphous regions than those present in pure PVA films.

In conclusion, 4% U-CQDs synthesized at 180 °C in the PVA matrix showed significantly enhanced rheological and mechanical strength. Meanwhile, the nitrogen-doped CQDs-reinforced PVA nanocomposite exhibited enhanced antibacterial properties due to the higher absorption of light. Thus, these materials can find applications in textile warp sizing and minimize the consumption of sizing materials. Moreover, U-CQDs can suppress the UV degradation of PVA used for outdoor applications.

Data availability

Data will be available upon request.

Author contributions

Conceptualization, Z. K. and M. A.; formal analysis, Z. L., U. K. and K. S.; funding acquisition, H. B. A. and M. J.; investigation, M. B. Q. and A. S. A.; project administration, M. B. Q. and Z. K.; resources, M. J. and H. B. A.; software, U. K. and K. S.; validation, S. N. A.; writing original draft, Z. L. and M. A.; writing review & editing, M. B. Q. and Z. K. All authors have read and agreed to the publication.

Conflicts of interest

All authors certify that they have NO affiliations with or involvement in any organization or entity with any financial interest (such as honoraria; educational grants; participation in speakers' bureaus; membership, employment, consultancies, stock ownership, or other equity interest; and expert testimony or patent-licensing arrangements), or non-financial interest (such as personal or professional relationships, affiliations, knowledge or beliefs) in the subject matter or materials discussed in this manuscript.

Acknowledgements

References

1 Z. Latif, M. Ali, E. J. Lee, Z. Zubair and K. H. Lee, "Thermal and Mechanical Properties of Nano-Carbon-Reinforced Polymeric Nanocomposites: A Review", *J. Compos. Sci.*, 2023, 7(10), 441, DOI: **10.3390/JCS7100441**.

2 Z. Latif, K. Shahid, H. Anwer, R. Shahid, M. Ali, K. H. Lee and M. Alshareef, Carbon quantum dots (CQDs)-modified polymers: a review of non-optical applications, *Nanoscale*, 2024, **16**, 2265–2288, DOI: **10.1039/D3NR04997C**.

3 M. J. Molaei, "A review on nanostructured carbon quantum dots and their applications in biotechnology, sensors, and chemiluminescence", *Talanta*, 2019, **196**, 456–478, DOI: **10.1016/j.talanta.2018.12.042**.

4 B. K. John, S. Mathew, N. John, J. Mathew and B. Mathew, "Hydrothermal synthesis of N,S-doped carbon quantum dots as a dual mode sensor for azo dye tartrazine and fluorescent ink applications", *J. Photochem. Photobiol., A*, 2023, **436**, 114386, DOI: **10.1016/j.jphotochem.2022.114386**.

5 B. D. Latha, *et al.*, "Fluorescent carbon quantum dots for effective tumor diagnosis: A comprehensive review", *Biomed. Eng. Adv.*, 2023, **5**, 100072, DOI: **10.1016/j.bea.2023.100072**.

6 J. Chen, Z. Zhang and H. Lu, "Structure design and properties investigation of Bi2O2Se/graphene van der Waals heterojunction from first-principles study", *Surf. Interfaces*, 2022, **33**, 102289, DOI: **10.1016/J.SURFIN.2022.102289**.

7 A. Chaudhuri, K. K. Sandha, A. K. Agrawal, and P. N. Gupta, Introduction to smart polymers and their application, in *Smart Polymeric Nano-Constructs in Drug Delivery*, Elsevier, 2023, pp. 1–46, DOI: **10.1016/B978-0-323-91248-8.00002-7**.

8 G. Yang, Q. OuYang, J. Ye and L. Liu, "Improved tensile and single-lap-shear mechanical-electrical response of epoxy composites reinforced with gridded nano-carbons",

Composites, Part A, 2022, **152**, 106712, DOI: 10.1016/j.compositesa.2021.106712.

9 P. Sati, A. Verma, A. Zindal, S. Chauhan and V. K. Singh, "PVA biopolymer-acidic functionalized graphene hybrid nano composite for vibration isolation application: An experimental approach with variable reflux and vacuum timings", *Chem. Phys. Impact*, 2023, **6**, 100212, DOI: 10.1016/J.CHPHI.2023.100212.

10 N. Bisht, *et al.*, "Effect of functionalized silicon carbide nano-particles as additive in cross-linked PVA based composites for vibration damping application", *J. Vinyl Addit. Technol.*, 2021, **27**(4), 920–932, DOI: [10.1002/VNL.21865](10.1002/VNL.21865).

11 J. Bai, *et al.*, "High-performance thermoplastic polyurethane elastomer/carbon dots bulk nanocomposites with strong luminescence", *High Perform. Polym.*, 2020, **32**(7), 857–867, DOI: [10.1177/0954008320907123](10.1177/0954008320907123).

12 Y. Chen, S. Sun, T. Zhang, X. Zhou and S. Li, "Effects of post-weld heat treatment on the microstructure and mechanical properties of laser-welded NiTi/304SS joint with Ni filler", *Mater. Sci. Eng.*, 2020, **771**, 138545, DOI: 10.1016/J.MSEA.2019.138545.

13 J. Zhu, *et al.*, "Engineering cross-linking by coal-based graphene quantum dots toward tough, flexible, and hydrophobic electrospun carbon nanofiber fabrics", *Carbon*, 2018, **129**, 54–62, DOI: 10.1016/j.carbon.2017.11.071.

14 A. G. El-Shamy, "Novel conducting PVA/Carbon quantum dots (CQDs) nanocomposite for high anti-electromagnetic wave performance", *J. Alloys Compd.*, 2019, **810**, 151940, DOI: 10.1016/j.jallcom.2019.151940.

15 A. G. El-Shamy, "Composite (PVA/Cu nano) films: Two yield points, embedding mechanism and thermal properties", *Prog. Org. Coat.*, 2019, **127**, 252–259, DOI: 10.1016/j.porgcoat.2018.11.024.

16 L. Wang, *et al.*, "Enhancing the thermostability, UV shielding and antimicrobial activity of transparent chitosan film by carbon quantum dots containing N/P", *Carbohydr. Polym.*, 2022, **278**, 118957, DOI: 10.1016/j.carbpol.2021.118957.

17 D. Qin, *et al.*, "Ultra-high gas barrier and enhanced mechanical properties of corn cellulose nanocomposite films filled with graphene oxide nanosheets", *Carbohydr. Polym. Technol. Appl*, 2021, **2**, 100066, DOI: 10.1016/j.carpta.2021.100066.

18 A. Madhi, "Smart epoxy/polyurethane/carbon quantum dots hybrid coatings: Synthesis and study of UV-shielding, viscoelastic, and anti-corrosive properties", *Polym.-Plast. Technol. Mater.*, 2023, **62**(4), 403–418, DOI: [10.1080/25740881.2022.2116342](10.1080/25740881.2022.2116342).

19 M. Ali, A. S. Anjum, A. Bibi, S. Wageh, K. C. Sun and S. H. Jeong, "Gradient heating-induced bi-phase synthesis of carbon quantum dots (CQDs) on graphene-coated carbon cloth for efficient photoelectrocatalysis", *Carbon*, 2022, **196**, 649–662, DOI: 10.1016/j.carbon.2022.05.040.

20 W. Li, *et al.*, "Efficient photocathodic protection of nanoflower MgIn2S4-modified CNNs composites on 316 SS under visible light", *Mater. Res. Bull.*, 2024, **173**, 112694, DOI: 10.1016/J.MATERRESBULL.2024.112694.

21 H. Ding, S.-B. Yu, J.-S. Wei and H.-M. Xiong, "Full-Color Light-Emitting Carbon Dots with a Surface-State-Controlled Luminescence Mechanism", *ACS Nano*, 2016, **10**(1), 484–491, DOI: 10.1021/acsnano.5b05406.

22 S. Sun, L. Zhang, K. Jiang, A. Wu and H. Lin, "Toward High-Efficient Red Emissive Carbon Dots: Facile Preparation, Unique Properties, and Applications as Multifunctional Theranostic Agents", *Chem. Mater.*, 2016, **28**(23), 8659–8668, DOI: 10.1021/acs.chemmater.6b03695.

23 D. Chen, W. Wu, Y. Yuan, Y. Zhou, Z. Wan and P. Huang, "Intense multi-state visible absorption and full-color luminescence of nitrogen-doped carbon quantum dots for blue-light-excitable solid-state-lighting", *J. Mater. Chem. C*, 2016, **4**(38), 9027–9035, DOI: [10.1039/C6TC02853E](10.1039/C6TC02853E).

24 Y. Yan, *et al.*, "Systematic Bandgap Engineering of Graphene Quantum Dots and Applications for Photocatalytic Water Splitting and CO 2 Reduction", *ACS Nano*, 2018, **12**(4), 3523–3532, DOI: 10.1021/acsnano.8b00498.

25 S. H. Jin, D. H. Kim, G. H. Jun, S. H. Hong and S. Jeon, "Tuning the Photoluminescence of Graphene Quantum Dots through the Charge Transfer Effect of Functional Groups", *ACS Nano*, 2013, **7**(2), 1239–1245, DOI: [10.1021/nn304675g](10.1021/nn304675g).

26 K. Shahid, M. Alshareef, M. Ali, M. I. Yousaf, M. M. Alsowayigh and I. A. Khan, "Direct Growth of Nitrogen-Doped Carbon Quantum Dots on Co9S8 Passivated on Cotton Fabric as an Efficient Photoelectrode for Water Treatment", *ACS Omega*, 2023, **8**(44), 41064–41076, DOI: 10.1021/ACSOMEGA.3C03407/SUPPL_FILE/AO3C03407_SI_001.

27 Y. Zhang, X. Liu, M. Song and Z. Qin, "Tuning the Red-to-Green-Upconversion Luminescence Intensity Ratio of Na3ScF6: 20% Yb3+, 2% Er3+ Particles by Changes in Size", *Materials*, 2023, **16**(6), 2247, DOI: [10.3390/MA16062247](10.3390/MA16062247).

28 S. Zhu, Y. Song, X. Zhao, J. Shao, J. Zhang and B. Yang, "The photoluminescence mechanism in carbon dots (graphene quantum dots, carbon nanodots, and polymer dots): current state and future perspective", *Nano Res.*, 2015, **8**(2), 355–381, DOI: [10.1007/s12274-014-0644-3](10.1007/s12274-014-0644-3).

29 P. Zhu, K. Tan, Q. Chen, J. Xiong and L. Gao, "Origins of Efficient Multiemission Luminescence in Carbon Dots", *Chem. Mater.*, 2019, **31**(13), 4732–4742, DOI: 10.1021/acs.chemmater.9b00870.

30 S. Hu, Q. Chang, K. Lin and J. Yang, "Tailoring surface charge distribution of carbon dots through heteroatoms for enhanced visible-light photocatalytic activity", *Carbon*, 2016, **105**, 484–489, DOI: 10.1016/j.carbon.2016.04.078.

31 X. Li, S. Zhang, S. A. Kulinich, Y. Liu and H. Zeng, "Engineering surface states of carbon dots to achieve controllable luminescence for solid-luminescent composites and sensitive Be2+ detection", *Sci. Rep.*, 2014, **4**(1), 4976, DOI: 10.1038/srep04976.

32 Y. Zhou, *et al.*, "Size-dependent photocatalytic activity of carbon dots with surface-state determined

photoluminescence", *Appl. Catal., B*, 2019, **248**, 157–166, DOI: **10.1016/j.apcatb.2019.02.019**.

33 A. Madhi and B. Shirkavand Hadavand, "Fluorescent epoxy-graphene quantum dots nanocomposites: synthesis and study of properties", *Polym.-Plast. Technol. Mater.*, 2022, **61**(2), 117–130, DOI: **10.1080/25740881.2021.1959929**.

34 K. Yang, J. Guan, Z. Shao and R. O. Ritchie, "Mechanical properties and toughening mechanisms of natural silkworm silks and their composites", *J. Mech. Behav. Biomed. Mater.*, 2020, **110**, 103942, DOI: **10.1016/J.JMBBM.2020.103942**.

35 J. Mohammadian, B. Shirkavand Hadavand and S. Khajenoori, "Synthesis and Investigation on Viscoelastic Properties of Urethane Acrylate-Polyaniline", *Prog. Color, Color. Coat.*, 2018, **11**(4), 241–252, DOI: **10.30509/pccc.2018.80275**.

36 X. Du, C. Wang, G. Wu and S. Chen, "The Rapid and Large-Scale Production of Carbon Quantum Dots and their Integration with Polymers", *Angew. Chem., Int. Ed.*, 2021, **60**(16), 8585–8595, DOI: **10.1002/anie.202004109**.

37 D. Qin, *et al.*, "Ultra-high gas barrier and enhanced mechanical properties of corn cellulose nanocomposite films filled with graphene oxide nanosheets", *Carbohydr. Polym. Technol. Appl*, 2021, **2**, 100066, DOI: **10.1016/j.carpta.2021.100066**.

38 B. Sui, Y. Li and B. Yang, "Nanocomposite hydrogels based on carbon dots and polymers", *Chin. Chem. Lett.*, 2020, **31**(6), 1443–1447, DOI: **10.1016/j.cclet.2019.08.023**.

39 B. De, B. Voit and N. Karak, "Carbon dot reduced Cu 2 O nanohybrid/hyperbranched epoxy nanocomposite: mechanical, thermal and photocatalytic activity", *RSC Adv.*, 2014, **4**(102), 58453–58459, DOI: **10.1039/C4RA11120F**.

40 B. De, B. Voit and N. Karak, "Transparent Luminescent Hyperbranched Epoxy/Carbon Oxide Dot Nanocomposites with Outstanding Toughness and Ductility", *ACS Appl. Mater. Interfaces*, 2013, **5**(20), 10027–10034, DOI: **10.1021/am402415g**.

41 B. Ghosh, S. Gogoi, S. Thakur and N. Karak, "Bio-based waterborne polyurethane/carbon dot nanocomposite as a surface coating material", *Prog. Org. Coat.*, 2016, **90**, 324–330, DOI: **10.1016/j.porgcoat.2015.10.025**.

42 J. Bai, *et al.*, "High-performance thermoplastic polyurethane elastomer/carbon dots bulk nanocomposites with strong luminescence", *High Perform. Polym.*, 2020, **32**(7), 857–867, DOI: **10.1177/0954008320907123**.

43 L. Wang, *et al.*, "Enhancing the thermostability, UV shielding and antimicrobial activity of transparent chitosan film by carbon quantum dots containing N/P", *Carbohydr. Polym.*, 2022, **278**, 118957, DOI: **10.1016/j.carbpol.2021.118957**.

44 L. Kong, Y. Zhu, G. Huang and J. Wu, "Carbon nanodots as dual role of crosslinking and reinforcing chloroprene rubber", *Compos. Commun.*, 2020, **22**, 100441, DOI: **10.1016/j.coco.2020.100441**.

45 K. Ghosal, M. Kováčová, P. Humpolíček, J. Vajďák, M. Bodík and Z. Špitalský, "Antibacterial photodynamic activity of hydrophobic carbon quantum dots and polycaprolactone based nanocomposite processed *via* both electrospinning and solvent casting method", *Photodiagn. Photodyn. Ther.*, 2021, **35**, 102455, DOI: **10.1016/j.pdpdt.2021.102455**.

46 K. Ghosal, M. Kováčová, P. Humpolíček, J. Vajďák, M. Bodík and Z. Špitalský, "Antibacterial photodynamic activity of hydrophobic carbon quantum dots and polycaprolactone based nanocomposite processed *via* both electrospinning and solvent casting method", *Photodiagn. Photodyn. Ther.*, 2021, **35**, 102455, DOI: **10.1016/j.pdpdt.2021.102455**.

47 M. Ali, A. S. Anjum, R. Riaz, A. Bibi, K. C. Sun and S. H. Jeong, "Unraveling the surface states related Stokes shift dependent electrocatalytic activity of N-doped carbon quantum dots for photovoltaic applications", *Carbon*, 2021, **181**, 155–168, DOI: **10.1016/j.carbon.2021.04.075**.

48 Y. Chong, *et al.*, "Crossover between Anti- and Pro-oxidant Activities of Graphene Quantum Dots in the Absence or Presence of Light", *ACS Nano*, 2016, **10**(9), 8690–8699, DOI: **10.1021/acsnano.6b04061**.

49 M. Kováčová, *et al.*, "Carbon Quantum Dots Modified Polyurethane Nanocomposite as Effective Photocatalytic and Antibacterial Agents", *ACS Biomater. Sci. Eng.*, 2018, **4**(12), 3983–3993, DOI: **10.1021/acsbiomaterials.8b00582**.

50 N. A. Travlou, D. A. Giannakoudakis, M. Algarra, A. M. Labella, E. Rodríguez-Castellón and T. J. Bandosz, "S- and N-doped carbon quantum dots: Surface chemistry dependent antibacterial activity", *Carbon*, 2018, **135**, 104–111, DOI: **10.1016/j.carbon.2018.04.018**.